Optica Applicata, Vol. LV, No. 4, 2025
DOI: 10.37190/oa/211820

Study of a tri-ring Er-doped fiber laser system: Stability, bifurcation, hyper-scroll attractor, and a path to hyperchaos

Senlin Yan

Department of Electronic Engineering, Nanjing Xiaozhuang University,
3601 Hongjing Avenue, Nanjing, China
e-mail: senlinyan@163.com

To develop a hyperchaotic laser generator, we designed and investigated a novel tri-ring Er-doped fiber laser system. The system was assembled from three single-ring Er-doped fiber lasers with two couplers, and a mathematical model was established using a set of six-dimensional nonlinear coupling equations. We mathematically deduced the function of the stable field of each single-ring laser as the pump varied, and presented distributions of the lasers' stable outputs. We theoretically analyzed the instability of the system using three sets of cubic relation expressions, which were verified by nonlinear function curves. It demonstrated the possible existence of a twin-scroll strange attractor in each laser ring and a hyper-scroll strange attractor in the assembled tri-ring laser system, which was consistent with our numerical result. We found that, as a subsystem, each single -ring laser could maintain its nonlinear dynamics, while the assembled tri-ring system exhibited rich nonlinear dynamic behaviors, such as quasi-periodicity, bifurcation, chaos, and hyperchaos. Lyapunov exponents were used to characterize the system's dynamic behavior, while fractal dimensions were used to investigate the spatial construction of the dynamics within the system. In the numerical analysis, we evaluated the evolution of the system, starting at a stable state, passing from a quasi-period state, and developing into chaos. This revealed a path to chaos and hyperchaos through a bifurcation scenario by shifting one parameter of the system. Chaotic, stable, and double -periodic bifurcation regions were found after exploring a path to chaos after bifurcation by adjusting the pump level of each laser ring. Two chaotic regions and double-periodic regions were observed when exploring a path toward or away from chaos by adding the coupling level of two rings. Chaotic, stable, and double-periodic bifurcation regions were found after exploring a path toward or away from chaos by varying the gain coefficient and decay rate, respectively. We also found that hyperchaotic waves were accompanied by hyperchaotic moving orbits in the dynamic phase. The strange attractor was characterized by ergodicity, the real-time wave by both complexity and randomness, and the hyperchaotic signal by the wide-band spectrum. The power spectrum clearly revealed the hyperchaotic response, exhibiting numerous frequency peaks that were randomly distributed with varying amplitudes. The assembled tri-ring laser system demonstrated extensive application potential and significant research value in the fields of fiber laser technology, laser chaos, optical secure communication, optical random signal generator, and laser radar.

Keywords: laser chaos, hyperchaos, bifurcation, Er-doped fiber laser.

1. Introduction

Laser systems often display many nonlinear optical phenomena, including stochastic oscillation and chaos [1-4]. Laser chaos exhibits random dynamics, and its dynamic behavior and output signals are difficult to predict because the system is highly sensitive to its starting conditions. The spectrum of a chaotic signal is characterized by broadband white noise. Therefore, chaotic signals of laser chaos have been widely used in spread communications, optical encoding, optical random signal generation, and optical radar [5-9]. Laser chaos has become a hotspot issue in laser technology, physics optics, and nonlinear optoelectronic devices [10-13]. To further promote the development of laser chaos technology and its applications, the invention of new laser chaos systems has become an important research focus. To date, chaotic laser systems mainly include external light injected laser systems, external cavity delayed feedback laser systems, modulating laser systems, and coupled laser systems [14-18]. The development of new types of laser chaos systems remains an important goal.

In recent years, fiber lasers have revolutionized various fields, such as optical communication, optical sensing, laser surgery, nonlinear optics, and optical materials [19-22]. An Er-doped fiber laser is a type of fiber laser that adopts an optical fiber as its gain medium and generates lasing by actively pumping rare earth erbium ions in the optical fiber. Er-doped fiber lasers are readily fused with fiber and can easily be integrated into fiber communication networks due to the compact size of their optical components and their minimal losses around 1550 nm. Thus, they are extensively used in optical fiber communication, fiber sensors, and fiber guidance [23,24]. Fiber lasers have important research value and unique significance in optics and laser physics because they contain a high concentration of erbium ions, provide high gain, produce high-quality light, and support a single transverse mode in which the electric field oscillates slowly for a period of 10 ms (in contrast, semiconductor lasers oscillate in short nanosecond periods) [22,25,26]. Fiber lasers have been reported to display irregular and random oscillations, such as undamped, stochastic, and chaotic oscillations. Chaotic fiber lasers can be used in secure communication, optical random signal generation, and laser radar systems [22,24-27].

In terms of dynamics, attractors readily arise in fiber lasers. The ability to control instability enables the selection of attractor types. By modulating the pump or cavity losses, fiber lasers can be induced to exhibit the coexistence of high-order periodic attractors. These attractors often differ in periodicity, with longer periods corresponding to higher pulse energies. High-power pulsing in fiber lasers has applications in cutting, surgery, and long-distance optical signal fiber transmission.

Recently, the dynamics of solitary Er-doped fiber lasers have been extensively studied [22,25,26]. However, there remains a need for comprehensive investigation into the dynamics of coupled Er-doped fiber lasers in different coupling configurations.

Two coupled fiber lasers have particularly piqued our interest, as this type of system offers ready control advantages, dual outputs, and the potential for chaos genera-

tion [28-31]. The dynamic behavior of such laser systems often follows a route to chaos through a series of Hopf bifurcations, resulting in period-one, quasi-periodic, and chaos states.

In nonlinear dynamics, Lyapunov exponents (LEs) are used to characterize dynamic system behavior. A single positive LE indicates chaos, while two or more positive LEs indicate hyperchaos. Currently, most reported chaotic laser systems have only one positive LE [1-4, 22, 25, 26]. Our study focuses on generating hyperchaotic behavior by extending previous research [32-35]. We constructed a novel tri-ring Er-doped fiber laser system to produce hyperchaos by coupling three single-ring lasers in a "ring–coupling–ring–coupling–ring" configuration.

Physically, the assembled system has the synthesized advantage of a simple single -ring laser subsystem forming a tri-ring double-coupling laser system with highly complex nonlinear interaction dynamics. Mathematically, the system dynamics are described by six sets of coupled nonlinear equations, introducing a high degree of freedom in both physical and mathematical space—a desirable attribute in high-dimensional chaotic systems. Such high-dimensional system outputs can enhance coding security in chaotic communication systems, as hyperchaotic behavior provides multiple secret keys [15, 19].

The two optical couplers generate the tri-ring laser system, which naturally arises from the phase shifts in signal propagation between subsystems. In these mutually interacting subsystems, coupling introduces two additional high-dimensional phase spaces and provides two new sources of possible instabilities, effectively creating an optical three-body problem. As a result, the system exhibits a wide range of dynamic behaviors, including self-pulsing, quasi-periodicity, bifurcation, chaos, and hyperchaos.

The following questions guide our study: How are nonlinear dynamic states distributed? What outcomes do their physical mechanisms lead to? How does the system operate, and how do the parameters dominate its dynamics? What are the advantages of this tri-ring configuration? Addressing these questions requires in-depth investigation.

In this paper, we explore the overall dynamics and nonlinear oscillation behaviors of the tri-ring Er-doped fiber laser system as the system parameters are varied. We focus on two key questions: How does the system transition to chaos and hyperchaos? How does it display different dynamic behaviors along this route? Addressing these questions provides valuable insight into the collective behaviors of the three laser rings and informs optimal laser parameters and configurations for improving performance. Using time series analysis, bifurcation diagrams, signal spectra, LEs, and fractal dimensions, we demonstrate that while the dynamics of individual rings may be similar, the assembled system exhibits distinctive characteristics inherent to its configuration.

We also theoretically analyze the stability properties of three single-ring lasers subjected to two bidirectional couplings. By examining nonlinear function curves, we study instabilities arising from bidirectional interactions and their entrainment properties. The study is conducted under the nondegenerate (different laser rings) and de-

generate (identical laser rings) conditions. This system's dynamics depend heavily on the subsystems, allowing us to study the relative behavior among the three rings. Key parameters include the pump (easily adjustable), coupling level (building parameter), gain coefficient, and decay rate (intrinsic laser parameters), which collectively dominate system dynamics.

We numerically investigate the stable regions of the tri-ring laser system in nonlinear dynamics and analyze the stable regions of each individual laser ring. From a numerical perspective, we examine the nonlinear dynamic behaviors of the assembled system, including bifurcation, chaos, and hyperchaos, by varying system parameters. In our simulations, we explore the onset of instability and the dynamic evolution process, beginning at stability, progressing through quasi-periodicity, and ultimately exhibiting chaos and hyperchaos. We also demonstrate a path to chaos and hyperchaos, starting from a period-one state and passing through a quasi-periodic bifurcation scenario as a system parameter is adjusted. Moreover, our results have extensive application value and research importance in the fields of fiber laser technology, chaotic laser emission, chaotic coding communication, optical random signal generation, and chaotic laser radar systems.

2. The tri-ring laser model

Figure 1 presents the design of our tri-ring Er-doped fiber laser system. Laser A (or ring a) is coupled to laser B (or ring b) by coupler C_1, and laser B is coupled to laser C (or ring c) by coupler C_2. In other words, the system is constructed by coupling one laser ring to two others, forming our "ring–coupling–ring–coupling–ring" configuration. When the electric field of one ring is injected into another through a coupler, a phase shift π arises between the two electric fields. The polarization variable can be ignored because the polarization decay rate (on the order of 10^{11}) is much higher than the decay rates of the population from the lasing upper level (on the order of 10^2) and the lasing field (on the order of 10^7). In this case, the dynamics of a single-ring Er-doped fiber laser are reduced to a two-dimensional dynamic model. The dynamics of each

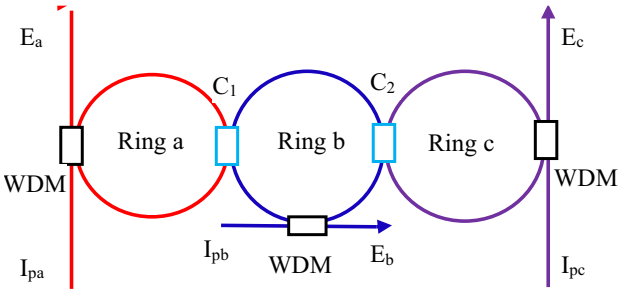

Fig. 1. A tri-ring Er-doped fiber laser system and its assembled subsystem. The couplers are represented by C_1 and C_2. The wavelength division multiplexer (WDM) is used for the pump injection and the laser output.

laser ring in the assembled system are described by the following normalized rate equations [30-33]:

$$\frac{\mathrm{d}}{\mathrm{d}t}E_\mathrm{a} = -k_\mathrm{a}(E_\mathrm{a} - \eta_0 E_\mathrm{b}) + g_\mathrm{a} E_\mathrm{a} D_\mathrm{a} \tag{1}$$

$$\frac{\mathrm{d}}{\mathrm{d}t}D_\mathrm{a} = -(1 + I_\mathrm{pa} + E_\mathrm{a}^2) D_\mathrm{a} + I_\mathrm{pa} - 1 \tag{2}$$

$$\frac{\mathrm{d}}{\mathrm{d}t}E_\mathrm{b} = -k_\mathrm{b}(E_\mathrm{b} + \eta_0 E_\mathrm{a} + \eta_0 E_\mathrm{c}) + g_\mathrm{b} E_\mathrm{b} D_\mathrm{b} \tag{3}$$

$$\frac{\mathrm{d}}{\mathrm{d}t}D_\mathrm{b} = -(1 + I_\mathrm{pb} + E_\mathrm{b}^2) D_\mathrm{b} + I_\mathrm{pb} - 1 \tag{4}$$

$$\frac{\mathrm{d}}{\mathrm{d}t}E_\mathrm{c} = -k_\mathrm{c}(E_\mathrm{c} - \eta_0 E_\mathrm{b}) + g_\mathrm{c} E_\mathrm{c} D_\mathrm{c} \tag{5}$$

$$\frac{\mathrm{d}}{\mathrm{d}t}D_\mathrm{c} = -(1 + I_\mathrm{pc} + E_\mathrm{c}^2) D_\mathrm{c} + I_\mathrm{pc} - 1 \tag{6}$$

In these equations, subscripts a, b, and c represent laser rings a, b, and c, respectively. E denotes the electric field, and D represents the population inversions inside the laser ring, where it was normalized by the total populations. I_p is the pump intensity in the laser ring, expressed as $\tau_2 W_\mathrm{p}$, where W_p represents the pump level, and τ_2 is the decay time of the population at the lasing upper level (approximately 10 ms). Time t is normalized by τ_2, η_0 is the coupling coefficient, k is the decay rate, and g is the gain coefficient.

3. Dynamics

3.1. Instability

In nonlinear physics, instability is often related to the presence of multiple stable points in a system. Mathematically, the roots of the fixed points of the system have three real solutions or at least two real solutions. Under such conditions, instability arises in the system. From a perspective of nonlinear functions, we begin our analysis of system instability. To describe the fixed states of Eqs. (1)–(6), the fixed points are derived as follows:

$$-k_\mathrm{a}(E_\mathrm{a0} - \eta_0 E_\mathrm{b0}) + g_\mathrm{a} E_\mathrm{a0} \frac{I_\mathrm{pa} - 1}{1 + I_\mathrm{pa} + E_\mathrm{a0}^2} = 0 \tag{7}$$

$$-k_\mathrm{b}(E_\mathrm{b0} + \eta_0 E_\mathrm{a0} + \eta_0 E_\mathrm{c0}) + g_\mathrm{b} E_\mathrm{b0} \frac{I_\mathrm{pb} - 1}{1 + I_\mathrm{pb} + E_\mathrm{b0}^2} = 0 \tag{8}$$

$$-k_{\mathrm{c}}(E_{\mathrm{c}0}-\eta_0 E_{\mathrm{b}0})+g_{\mathrm{c}}E_{\mathrm{c}0}\frac{I_{\mathrm{pc}}-1}{1+I_{\mathrm{pc}}+E_{\mathrm{c}0}^2}=0 \tag{9}$$

where subscript 0 indicates a fixed point. Equations (7)–(9) are also rewritten as follows:

$$E_{\mathrm{a}0}^3+E_{\mathrm{a}0}^2G_{\mathrm{a}}+E_{\mathrm{a}0}Q_{\mathrm{a}}+R_{\mathrm{a}}=0 \tag{10}$$

$$E_{\mathrm{b}0}^3+E_{\mathrm{b}0}^2G_{\mathrm{b}}+E_{\mathrm{b}0}Q_{\mathrm{b}}+R_{\mathrm{b}}=0 \tag{11}$$

$$E_{\mathrm{c}0}^3+E_{\mathrm{c}0}^2G_{\mathrm{c}}+E_{\mathrm{c}0}Q_{\mathrm{c}}+R_{\mathrm{c}}=0 \tag{12}$$

where

$$G_{\mathrm{a}}=-\eta_0 E_{\mathrm{b}0}$$

$$Q_{\mathrm{a}}=-\frac{g_{\mathrm{a}}(I_{\mathrm{pa}}-1)-k_{\mathrm{a}}(1+I_{\mathrm{pa}})}{k_{\mathrm{a}}}$$

$$R_{\mathrm{a}}=-\eta_0 E_{\mathrm{b}0}(1+I_{\mathrm{pa}})$$

$$G_{\mathrm{b}}=\eta_0 E_{\mathrm{a}0}+\eta_0 E_{\mathrm{c}0}$$

$$Q_{\mathrm{b}}=\frac{k_{\mathrm{b}}(1+I_{\mathrm{pb}})-g_{\mathrm{b}}(I_{\mathrm{pb}}-1)}{k_{\mathrm{b}}}$$

$$R_{\mathrm{b}}=(\eta_0 E_{\mathrm{a}0}+\eta_0 E_{\mathrm{c}0})(1+I_{\mathrm{pb}})$$

$$G_{\mathrm{c}}=-\eta_0 E_{\mathrm{b}0}$$

$$Q_{\mathrm{c}}=-\frac{g_{\mathrm{c}}(I_{\mathrm{pc}}-1)-k_{\mathrm{c}}(1+I_{\mathrm{pc}})}{k_{\mathrm{c}}}$$

$$R_{\mathrm{c}}=-\eta_0 E_{\mathrm{b}0}(1+I_{\mathrm{pc}})$$

For example, when laser B produces a stable output $E_{\mathrm{b}0}$, there is the possibility of three roots in Eq. (10), which implies the existence of instability, as the laser cannot lock onto a single stable point because no one fixed point can be assumed to be more dominant than the others. We set the following:

$$\hat{p}_1=\frac{1}{3}Q_{\mathrm{a}}-\frac{1}{9}G_{\mathrm{a}}^2,\qquad \hat{q}_1=\frac{1}{27}G_{\mathrm{a}}^3-\frac{1}{6}G_{\mathrm{a}}Q_{\mathrm{a}}+\frac{1}{2}R_{\mathrm{a}}$$

$$\hat{p}_2 = \frac{1}{3}Q_b - \frac{1}{9}G_b^2, \quad \hat{q}_2 = \frac{1}{27}G_b^3 - \frac{1}{6}G_b Q_b + \frac{1}{2}R_b$$

$$\hat{p}_3 = \frac{1}{3}Q_c - \frac{1}{9}G_c^2, \quad \hat{q}_3 = \frac{1}{27}G_c^3 - \frac{1}{6}G_c Q_c + \frac{1}{2}R_c$$

Letting $E_{a0,\,b0,\,c0} = X - G_{a,\,b,\,c}$, Eqs. (10)–(12) are then rewritten as follows:

$$X^3 + 3X^2\hat{p}_{1,\,2,\,3} + 2\hat{q}_{1,\,2,\,3} = 0 \tag{13}$$

We discussed only the real roots of Eq. (13):

i) When $q_{1,\,2,\,3}^2 + p_{1,\,2,\,3}^3 < 0$, there are three differential real roots of Eq. (13):

$$X_1 = 2\sqrt{-\hat{p}_{1,\,2,\,3}}\cos\left(\frac{1}{3}\xi_{1,\,2,\,3}\right)$$

$$X_2 = 2\sqrt{-\hat{p}_{1,\,2,\,3}}\cos\left(\frac{1}{3}\xi_{1,\,2,\,3} + \frac{2}{3}\pi\right)$$

$$X_3 = 2\sqrt{-\hat{p}_{1,\,2,\,3}}\cos\left(\frac{1}{3}\xi_{1,\,2,\,3} + \frac{4}{3}\pi\right)$$

where

$$\cos\xi_{1,\,2,\,3} = \frac{\hat{q}_{1,\,2,\,3}}{\hat{p}_{1,\,2,\,3}\sqrt{-\hat{p}_{1,\,2,\,3}}}, \quad 0 < \xi_{1,\,2,\,3} < \pi$$

ii) When $q_{1,\,2,\,3}^2 + p_{1,\,2,\,3}^3 = 0$, there are two real roots of Eq. (13):

$$X_1 = 2\sqrt[3]{-\hat{q}_{1,\,2,\,3}}, \quad X_2 = X_3 = -\sqrt[3]{-\hat{q}_{1,\,2,\,3}}$$

Thus, we inferred the existence of instability in the system when $q_{1,\,2,\,3}^2 + p_{1,\,2,\,3}^3 \le 0$.

To verify this theory, we examined the stable output from each laser ring by numerically calculating Eqs. (7)–(9). A set of numerical results represents unstable regions, as shown in Fig. 2 (typical nonlinear function curves), indicating the possible occurrence of instability in the system. The parameters were set as $k_a = k_b = k_c = 1000$, $\eta_0 = 0.22$, $g_a = 10500$, $g_b = 10000$, and $g_c = 5800$. These nonlinear curve diagrams confirm the potential for instability under certain conditions.

We noted that significant instability is observed in the unstable region shown in Fig. 2(a) for lasers A and B (or Fig. 2(c) for lasers C and B) when perturbation from one laser is introduced to another laser. In this case, instability is inevitably triggered, leading to dynamic unstable states in the system. Thus, the assembled laser system displays the characteristics of an unstable element and can be used to fabricate an unstable

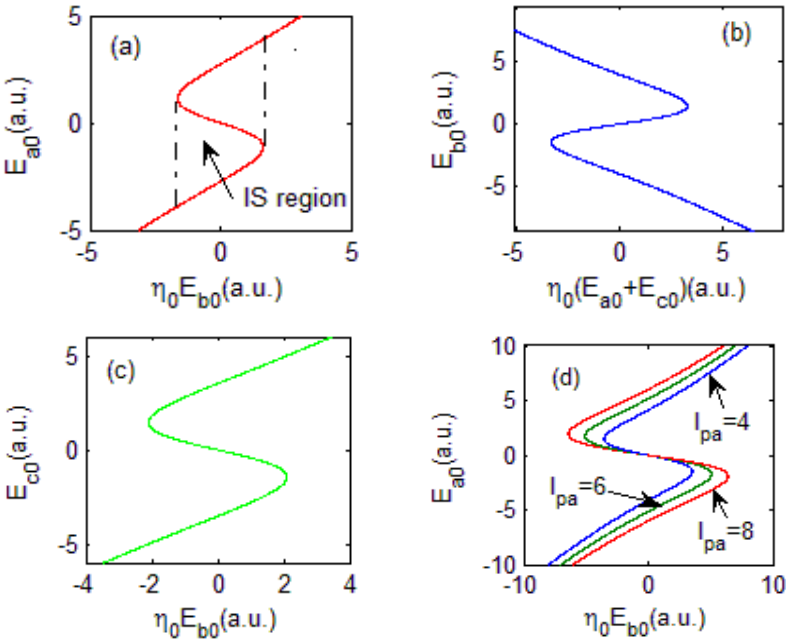

Fig. 2. Instability (IS): (a) $I_{pa} = 2$, (b) $I_{pb} = 3$, (c) $I_{pc} = 4$, and (d) with different pump levels.

optical oscillation device. Our numerical results are in agreement with our theoretical predictions.

3.2. The possibility of strange attractors and hyperchaos

The distribution of fixed points is one condition in mathematical space that can result in the appearance of strange attractors in the phase space of a nonlinear system. By examining the fixed points of the system in addition to the zero solution, we obtained another set of simple equations describing the fixed points as follows:

$$E_{a0} = \pm\sqrt{\frac{I_{pa}-1}{D_{a0}-(1+I_{pa})}} \tag{14}$$

$$E_{b0} = \pm\sqrt{\frac{I_{pb}-1}{D_{b0}-(1+I_{pb})}} \tag{15}$$

$$E_{c0} = \pm\sqrt{\frac{I_{pc}-1}{D_{c0}-(1+I_{pc})}} \tag{16}$$

where E_a, E_b, and E_c each have at least two sets of solutions (corresponding to a set of D_{a0}, D_{b0}, and D_{c0}), which indicates that each laser ring possesses at least two sets

of fixed points. As a result, the dynamic behavior of each laser moves stochastically around the two fixed points, since the second oscillation of the field in one ring is continuously stimulated by the field from another coupled laser ring. Because neither fixed point can be assumed to be more stable than the other, this becomes a necessary condition for the appearance of a twin-scroll strange attractor in the phase space of each laser ring. Thus, strange attractors may arise in the phase space of the individual rings. Since the system as a whole possesses at least six sets of fixed points in addition to the zero solution, its dynamics behave stochastically around these points under the same coupling mechanism. Consequently, we inferred the appearance of a hyper-scroll strange attractor in the assembled tri-ring laser system within the phase space of E_a, E_b, and E_c under certain conditions.

To verify the possibility of strange attractors, we examined the trajectories in the dynamic phase space of each laser ring by numerically solving Eqs. (1)–(6). Our results revealed the presence of twin-scroll strange attractors in the two-dimensional dynamic phase space of each laser ring, as well as a hyper-scroll strange attractor in the three-dimensional dynamic phase space formed by E_a, E_b, and E_c in the assembled tri-ring laser system, as shown in Fig. 3. The parameters were set as $k_a = k_b = k_c = 1000$, $\eta_0 = 0.2$, $g_a = 10500$, $g_b = 10000$, $g_c = 5800$, and $I_{pa} = I_{pb} = I_{pc} = 2$. In this case, the chaotic attractors are confirmed as strange attractors because the dynamics yield two positive LEs: 21.8 and 0.14. Our numerical results agree with our theoretical predictions.

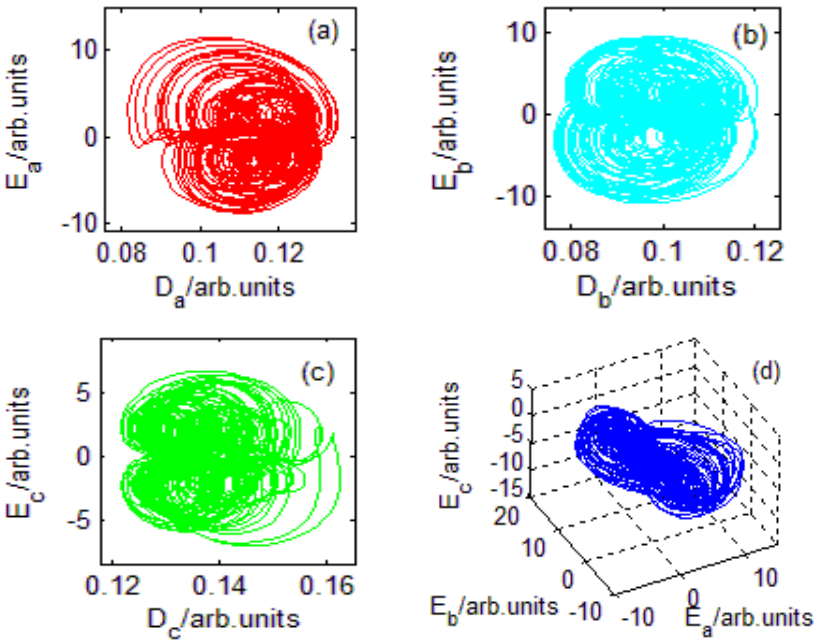

Fig. 3. Strange attractors in the dynamics of each laser ring (a, b, and c) and the full system (d).

3.3. Stable field distribution *versus* pump

For simplicity, we assumed that the three laser rings have the same parameters: $k_a = k_b = k_c = k$, $g_a = g_b = g_c = g$, and $I_{pa} = I_{pb} = I_{pc} = I_p$. Substituting these into Eq. (10), and considering the symmetry of Eqs. (7)–(9), while excluding the solution $E_{a0} = E_{c0} = E_{b0} = 0$, we obtained at least two sets of solutions: (i) $E_{a0} = -E_{c0}$, $E_{b0} = 0$; (ii) $E_{a0} = -E_{c0}$, $E_{b0} \neq 0$. Our discussion proceeds as follows.

i) When $E_{a0} = -E_{c0}$ and $E_{b0} = 0$ from Eqs. (10) and (12), we obtained the following:

$$E_{a0}^2 = \left(\frac{g}{k} - 1\right) I_p - \left(\frac{g}{k} + 1\right) \quad \text{or} \quad E_{a0\pm} = \pm\sqrt{\left(\frac{g}{k} - 1\right)(I_p - I_C)}$$

$$E_{c0}^2 = \left(\frac{g}{k} - 1\right) I_p - \left(\frac{g}{k} + 1\right) \quad \text{or} \quad E_{c0\mp} = \mp\sqrt{\left(\frac{g}{k} - 1\right)(I_p - I_C)}$$

where I_C represents the lowest limited pump of the fixed point existence, and its value is

$$I_C = \left(\frac{g}{k} + 1\right) / \left(\frac{g}{k} - 1\right)$$

ii) When $E_{a0} = -E_{c0}$ and $E_{b0} \neq 0$ from Eq. (11), we obtained the following:

$$E_{b0}^3 + E_{b0}^2 \widehat{G}_b + E_{b0} \widehat{Q}_b + \widehat{R}_b = 0 \tag{17}$$

where

$$\widehat{G}_b = \eta_0 E_{a0} + \eta_0 E_{c0} = 0$$

$$\widehat{Q}_b = (1 + I_p) - (I_p - 1)\frac{g}{k}$$

$$\widehat{R}_b = (\eta_0 E_{a0} + \eta_0 E_{c0})(1 + I_p) = 0$$

We obtained the root of Eq. (17) as follows:

$$E_{b0}^2 = \left(\frac{g}{k} - 1\right) I_p - \left(\frac{g}{k} + 1\right) \quad \text{or} \quad E_{b0\pm} = \pm\sqrt{\left(\frac{g}{k} - 1\right)(I_p - I_C)}$$

where

$$I_C = \left(\frac{g}{k} + 1\right) / \left(\frac{g}{k} - 1\right)$$

From Eq. (10), we obtained the following:

$$E_{a0}^3 + E_{a0}^2 b_\pm + E_{a0} c + d_\pm = 0 \tag{18}$$

where

$$b_{\pm} = -\eta_0 E_{\mathrm{b0}\pm}, \quad c = -\left[(I_{\mathrm{p}} - 1)\frac{g}{k} - (1 + I_{\mathrm{p}})\right], \quad d_{\pm} = -\eta_0 E_{\mathrm{b0}\pm}(1 + I_{\mathrm{p}})$$

We set $A_{\pm} = b_{\pm}^2 - 3c$, $B_{\pm} = b_{\pm} c - 9 d_{\pm}$, $C_{\pm} = c^2 - 3 b_{\pm} d_{\pm}$ and the discriminant as $\Delta_{\pm} = B_{\pm}^2 - 4 A_{\pm} C_{\pm}$.

We focused on the case in which Eq. (18) has three real roots when $\Delta_{\pm} < 0$. In this case, two sets of real roots are given as follows:

$$E_{\mathrm{a01}\pm} = -\frac{b_{\pm}}{3} - \frac{2\sqrt{A_{\pm}}}{3}\cos\frac{\varphi_{\pm}}{3} \tag{19a}$$

$$E_{\mathrm{a02}\pm} = -\frac{b_{\pm}}{3} + \frac{2\sqrt{A_{\pm}}}{3}\left(\cos\frac{\varphi_{\pm}}{3} + \sqrt{3}\cos\frac{\varphi_{\pm}}{3}\right) \tag{19b}$$

$$E_{\mathrm{a03}\pm} = -\frac{b_{\pm}}{3} + \frac{2\sqrt{A_{\pm}}}{3}\left(\cos\frac{\varphi_{\pm}}{3} - \sqrt{3}\sin\frac{\varphi_{\pm}}{3}\right) \tag{19c}$$

where

$$\varphi_{\pm} = \arccos\left(\frac{2 A_{\pm} b_{\pm} - 3 B_{\pm}}{2\sqrt{A_{\pm}^3}}\right)$$

Hence, we also obtained two sets of solutions of the three stable points of laser C as follows:

$$E_{\mathrm{c01}\pm} = \frac{b_{\pm}}{3} + \frac{2\sqrt{A_{\pm}}}{3}\cos\frac{\varphi_{\pm}}{3} \tag{20a}$$

$$E_{\mathrm{c02}\pm} = \frac{b_{\pm}}{3} - \frac{2\sqrt{A_{\pm}}}{3}\left(\cos\frac{\varphi_{\pm}}{3} + \sqrt{3}\sin\frac{\varphi_{\pm}}{3}\right) \tag{20b}$$

$$E_{\mathrm{c03}\pm} = \frac{b_{\pm}}{3} - \frac{2\sqrt{A_{\pm}}}{3}\left(\cos\frac{\varphi_{\pm}}{3} - \sqrt{3}\sin\frac{\varphi_{\pm}}{3}\right) \tag{20c}$$

where

$$\varphi_{\pm} = \arccos\left(\frac{2 A_{\pm} b_{\pm} - 3 B_{\pm}}{2\sqrt{A_{\pm}^3}}\right)$$

and $E_{\mathrm{c01}} = -E_{\mathrm{a01}}$, $E_{\mathrm{c02}} = -E_{\mathrm{a02}}$, and $E_{\mathrm{c03}} = -E_{\mathrm{a03}}$.

Thus, the stable field distribution of each laser varies according to the pump parameter. As an example, setting $k = 1000$, $g = 10000$, $\eta_0 = 0.2$, and $I_{\mathrm{p}} = 3$, the lowest limited pump of real fixed points is $I_{\mathrm{C}} = 11/9 = 1.2222$. Hence, only a set of distributions of the

three stable fields of lasers A, B, and C as (4, –4), (0, 0), and (–4, 4), respectively, are shown. Correspondingly, the distribution of D_0 is (0.1, 0.5, 0.1) (presuming $D_0 = D_{a0} = = D_{b0} = D_{c0}$). The numerical results are shown in Fig. 4 (E_0 is used to indicate E_{a0}, E_{b0}, and E_{c0}), where $k = 1000$, $g = 10000$, $\eta_0 = 0.2$, and I_p shifts from $I_C = 1.2222$ to 10.

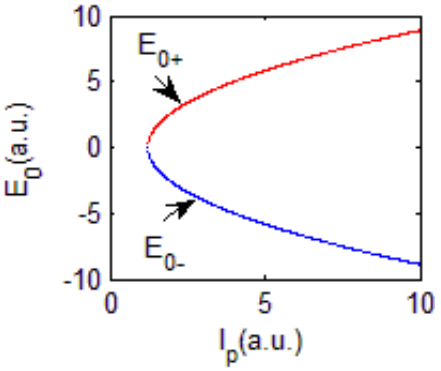

Fig. 4. Stable field distributions of each laser *versus* the pump.

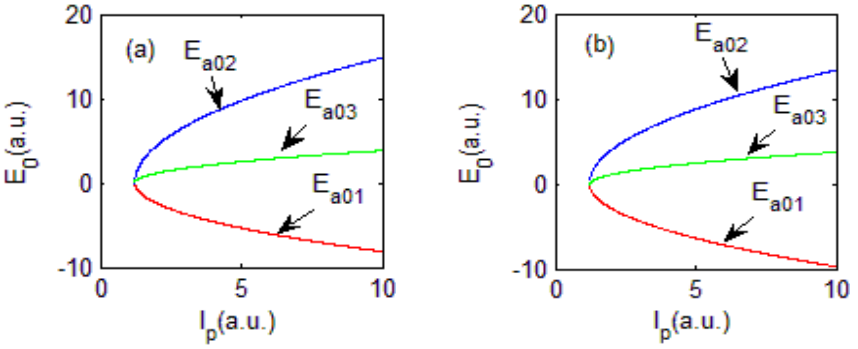

Fig. 5. Two sets of stable field distribution of laser A *versus* the pump when $E_0 = E_{b0+}$ using Eq. (19).

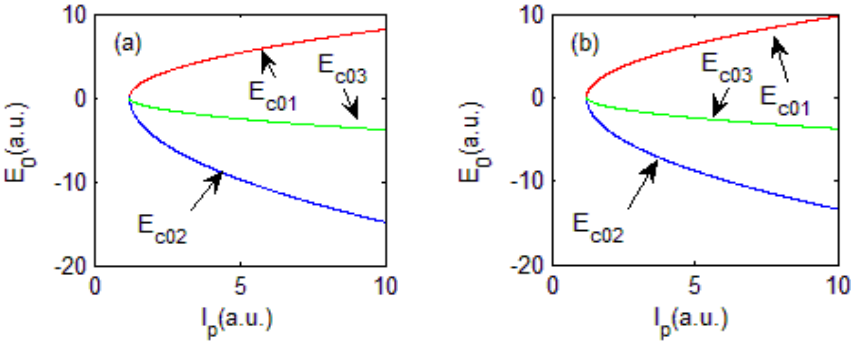

Fig. 6. Two sets of stable field distributions of laser C *versus* the pump when $E_0 = E_{b0-}$ using Eq. (20).

Another set of stable field distributions of lasers A, B, and C are shown in Figs. 4–6 (E_0 indicating the stable field of each laser, and not including $E_0 = 0$), where $k = 1000$, $g = 10000$, $\eta_0 = 0.2$, and I_p ranges from $I_C = 1.2222$ to 10.

4. Results and discussion

4.1. Bifurcation diagrams

A bifurcation diagram (or phase parametrization) is used to display the bifurcation process of a dynamic system by adjusting one parameter of the system, roughly describing the dynamic behavior of the system. Here, we numerically explored the dynamic evolution of the tri-ring laser system, starting from quasi-periodic behavior and progressing to chaos. We illustrated a path to chaos through period-doubling and quasi-bifurcation scenarios by adjusting system parameters. The bifurcation diagrams allow us to find chaotic, stable, double-periodic bifurcation, and other dynamic scenario regions. Our analysis considers how pump levels, coupling strength, decay rate, and gain impact system dynamics. We first examined pump levels *versus* output extrema in the parameter space. Then, we analyzed how coupling strength and intrinsic laser parameters (gain and decay rate) influence the output extrema. Such studies are crucial for optimizing the chaotic behavior of the system.

First, three sets of bifurcation diagrams are presented in Figs. 7–9, each showing a path to chaos as one pump parameter of the subsystem is varied. The vertical axis

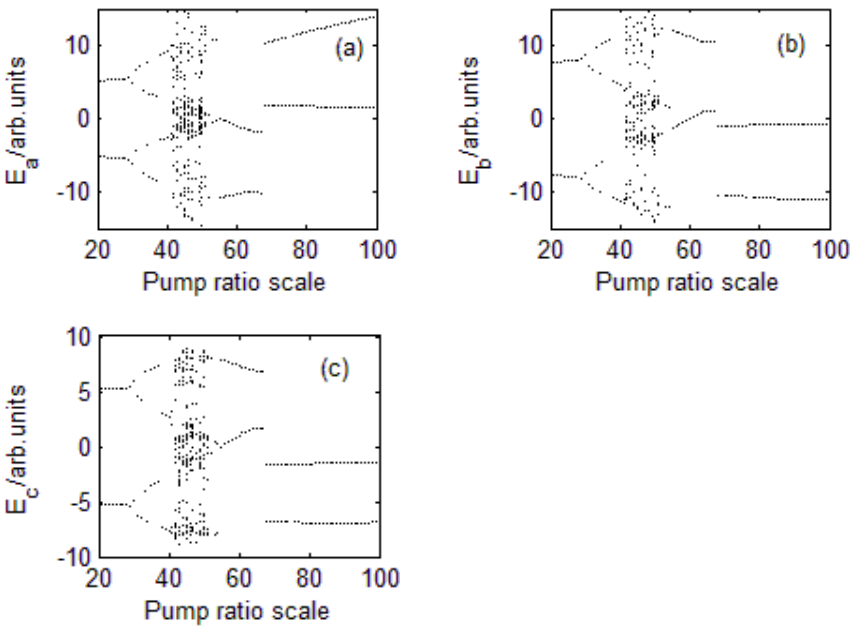

Fig. 7. Phase-parametrion *versus* the pump levels of laser A. (a) Laser A, (b) laser B, and (c) laser C.

represents the output extrema, and the horizontal axis represents the ratio scales of the pump levels. The normalized parameters of the tri-ring laser system are set as $\eta_0 = 0.22$, $k_a = k_b = k_c = 1000$, $g_a = 10500$, $g_b = 12000$, and $g_c = 5800$ [5-8]. When $I_{pb} = I_{pc} = 4$, the pump I_{pa} of laser A is varied from 1 to 8 in 100 equal steps, with the horizontal axis scaled from 20 to 100 to represent the ratio of pump levels. The results are shown in Fig. 7. After inspecting the phase-parametrion *versus* the pump levels of laser A, as well as a path to chaos after the one-periodic bifurcation, we found the following dynamic regions: the one-periodic region extends from 20 ($I_{pa} = 2.4$) to 27 ($I_{pa} = 2.89$), where self-pulsing or one-periodic oscillation occurs. The quasi-periodic bifurcation spans from 28 ($I_{pa} = 2.96$) to 42 ($I_{pa} = 3.94$), where quasi-periodic oscillations dominate. The chaotic region is observed between 43 ($I_{pa} = 4.01$) and 50 ($I_{pa} = 4.5$), where chaotic or stochastic oscillations occur. Beyond 51 ($I_{pa} = 4.57$), four-, three-, and double-periodic regions appear and persist up to 100 ($I_{pa} = 8$), indicating that the system moves away from chaos and transitions into stable period-doubled states as I_{pa} increases.

To show another path to chaos as pump I_{pb} varies, and to examine the system's sensibility to the pump and other parameters, we set another group of normalized parameters: $\eta_0 = 0.2$, $k_a = k_b = k_c = 1000$, $g_a = 10500$, $g_b = 10000$, and $g_c = 5800$ [5-8]. When $I_{pa} = I_{pc} = 2$, pump I_{pb} of laser B was varied from 1 to 10 in 100 equal steps, with the horizontal axis scaled from 20 to 100 to represent the ratio of pump levels. Figure 8 shows a path to chaos after one-periodic bifurcation. Three different regions were identified: the one-periodic region extends from 20 ($I_{pb} = 2.8$) to 33 ($I_{pb} = 3.97$). Then, chaotic and quasi-periodic regions appear alternately along the path, with the three main cha-

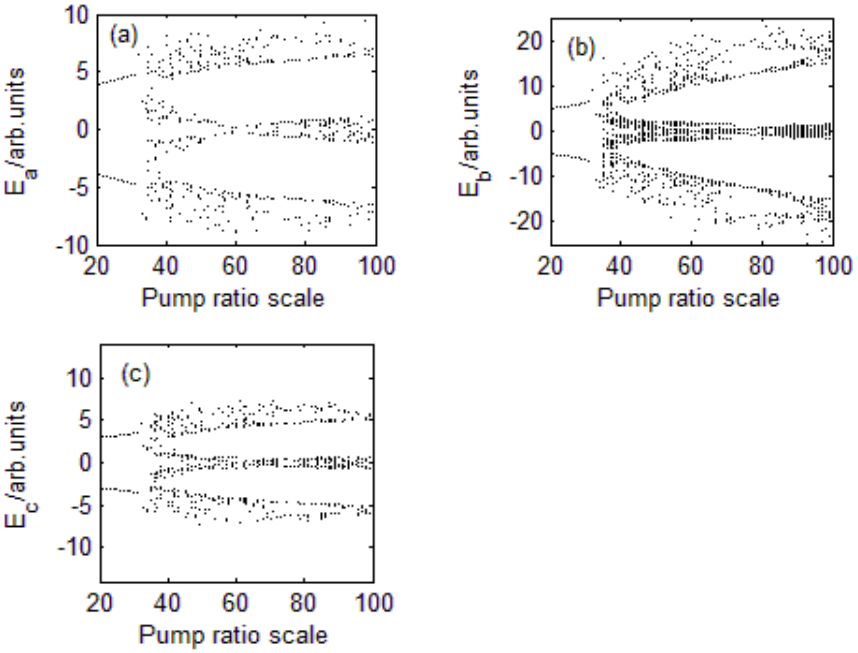

Fig. 8. Phase-parametrion *versus* the pump levels of laser B. (a) Laser A, (b) laser B, and (c) laser C.

otic intervals occurring from 34 (I_{pb} = 4.06) to 52 (I_{pb} = 4.68), from 58 (I_{pb} = 5.22) to 65 (I_{pb} = 6.85), and from 89 (I_{pb} = 9.01) to 10 (I_{pb} = 10). The quasi-periodic regions appear roughly from 67 (I_{pb} = 7.03) to 68 (I_{pb} = 7.12), from 74 (I_{pb} = 7.66) to 78 (I_{pb} = = 8.02), and at 88 (I_{pb} = 7.92).

The normalized parameters were set as η_0 = 0.2, $k_a = k_b = k_c$ = 1000, g_a = 10500, g_b = 12000, and g_c = 5800 [5-8]. When $I_{pa} = I_{pb}$ = 3, the pump I_{pc} of laser C was varied from 1 to 8 in 100 equal steps, with the horizontal axis was scaled from 20 to 100 to represent the ratio of pump levels. Figure 9 shows a path away from chaos passing through the quasi-periodic bifurcation evolution into the one-period, and the three different regions can be identified as follows: the chaotic region distributes from 20 (I_{pc} = 2.4) to 35 (I_{pc} = 3.45); the quasi-periodic bifurcation distributes from 36 (I_{pc} = 2.52) to 46 (I_{pc} = 3.22); the one-periodic region distributes from 47 (I_{pc} = 3.29) to 100 (I_{pc} = 8). The system moves away from chaos to enter a one-periodic state along the path with the addition of I_{pc}.

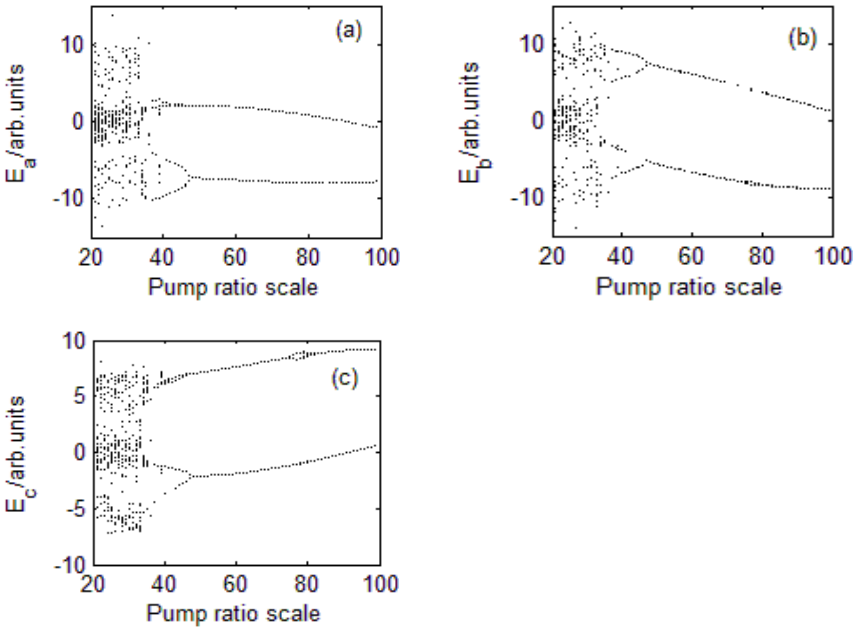

Fig. 9. Phase-parametrion *versus* the pump levels of laser C. (a) Laser A, (b) laser B, and (c) laser C.

We found that the pump strongly affects the path toward or away from chaos, with different pump levels producing different routes, and that the system showed high sensitivity to pump parameters. We also found that the chaotic zones shown in these paths are influenced not only by pump levels but also by coupling strength, decay rate, and gain. To further investigate the system's sensitivity to these parameters, we examined paths to chaos under varying coupling coefficients, gain, and decay rate. The results are shown in Figs. 10–12.

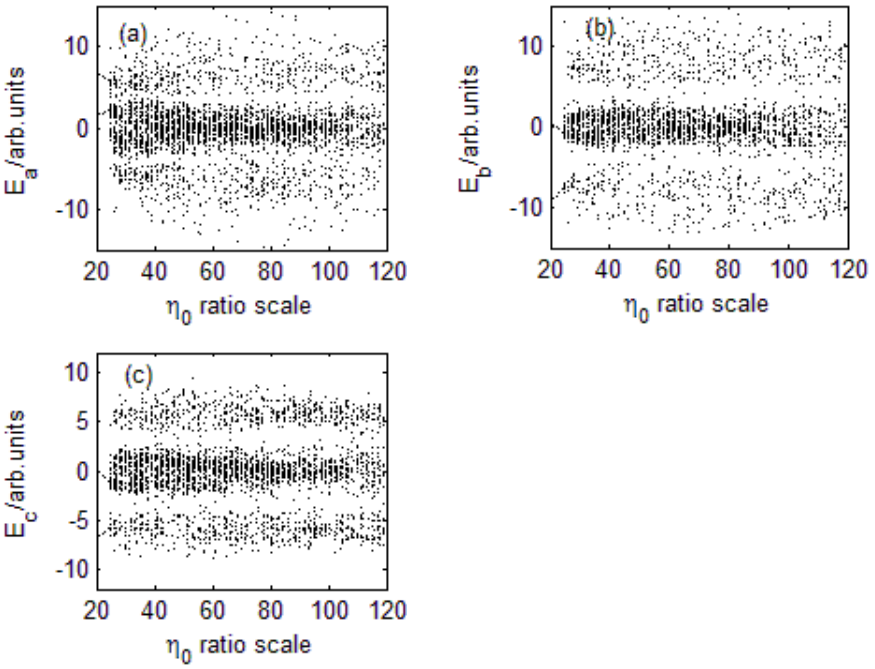

Fig. 10. Phase-parametrion *versus* the coupling coefficient. (a) Laser A, (b) laser B, and (c) laser C.

In this case, the normalized parameters were set to $k_a = k_b = k_c = 1000$, $g_a = 10500$, $g_b = 12000$, $g_c = 5800$, and $I_a = I_{pb} = I_{pc} = 3$. The coupling coefficient representing the coupling strength between lasers B and C was set at 0.22, while the coupling coefficient between lasers A and B η_0 was varied from 0.022 to 0.242 in 120 equal steps, with the horizontal axis scaled from 20 to 120. We found that the coupling coefficient can affect a path to chaos in the system. Figure 10 shows that the coupling coefficient strongly affects the path to chaos, producing a broad chaotic region between 27 ($\eta_0 = 0.0715$) and 120 ($\eta_0 = 0.242$). This result implies that coupling strength dominates the dynamics of the assembled system.

With another set of normalized parameters ($\eta_0 = 0.22$, $k_a = k_b = k_c = 1000$, $g_a = 10500$, $g_c = 5800$, $I_{pa} = I_{pb} = I_{pc} = 5$), the gain coefficient of laser B was varied to observe the system's response. Figure 11 shows a path to chaos emerging through quasi-periodic bifurcation as g_b increases from 5000 to 15000 in 100 equal steps, with the horizontal axis scaled from 20 to 80. Different regions can be identified: the chaotic region extends roughly from 50 ($g_b = 10000$) to 57 ($g_b = 10700$), while other regions include period-one, double-period, and other quasi-period intervals.

With the normalized parameters set as $\eta_0 = 0.22$, $k_a = k_c = 1000$, $g_a = 10500$, $g_b = = 12000$, $g_c = 5800$, and $I_{pa} = I_{pb} = I_{pc} = 3$, and the decay rate of laser B was varied to analyze system behavior. Figure 12 shows a path to chaos emerging through quasi-periodic bifurcation toward a one-periodic state as k_b increases from $0.2k$ to $1.6k$ ($k = 1000$)

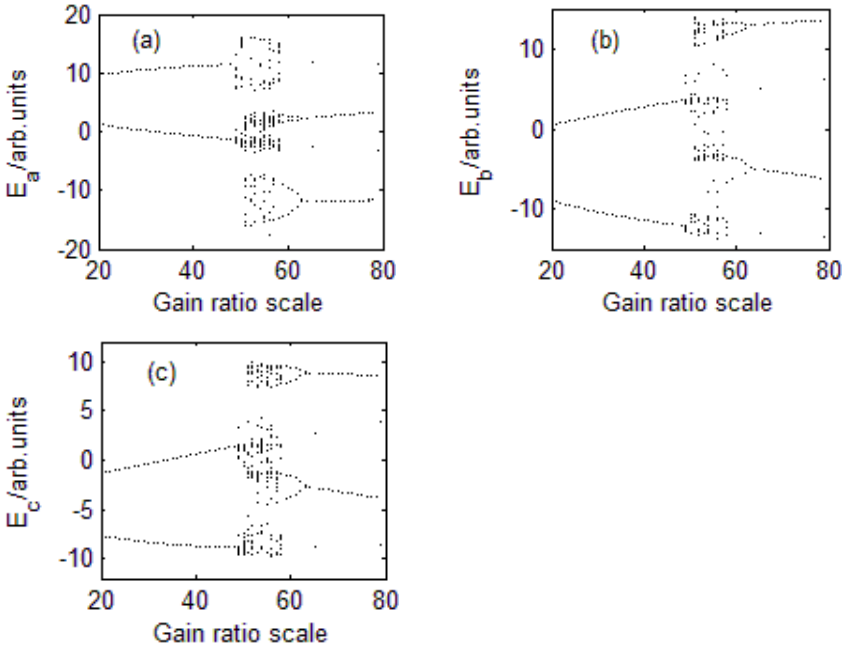

Fig. 11. Phase-parametrion *versus* the gain coefficient of laser B. (a) Laser A, (b) laser B, and (c) laser C.

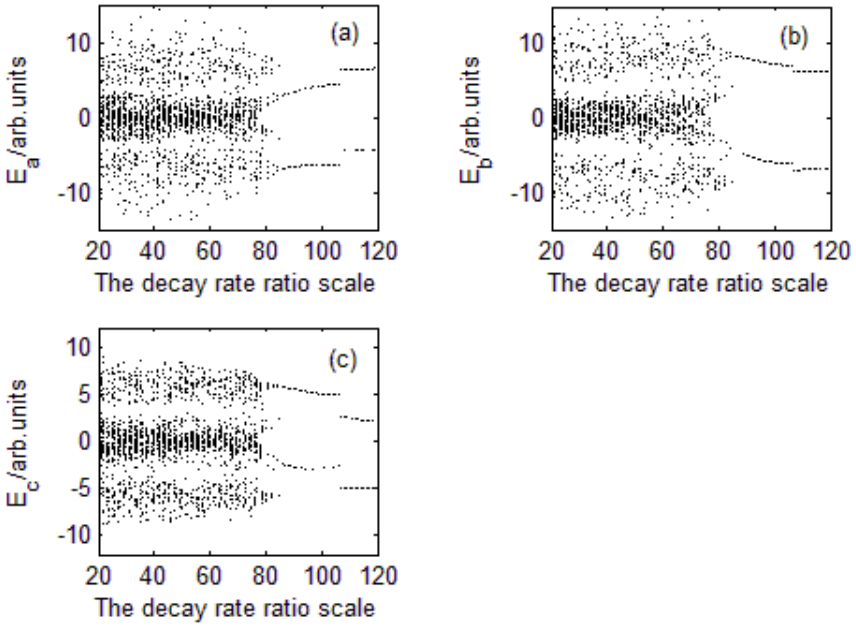

Fig. 12. Phase-parametrion *versus* the decay rate of laser B. (a) Laser A, (b) laser B, and (c) laser C.

in 120 equal steps, with the horizontal axis scaled from 20 to 120. Different regions can be identified: the chaotic region extends from 20 ($k_b = 0.3333k$) to 77 ($k_b = 1.0983k$); the quasi-periodic region extends from 78 ($k_b = 1.11k$) to 84 ($k_b = 1.18k$); and the one -periodic region extends from 85 ($k_b = 1.191k$) to 120 ($k_b = 1.6k$).

4.2. Lyapunov exponents and fractal dimensions

LEs and fractal dimensions are commonly used together to describe the dynamics and geometric characteristics of nonlinear dynamic systems. Fractal dimensions characterize the space occupied by the system's dynamics, while LEs are used to diagnose dynamic behavior, including quasi-bifurcations, by adjusting one system parameter. Numerical estimation of LEs can be achieved using long-term evolution of the Jacobian matrix or orbital perturbation methods (*e.g.*, the Wolf algorithm). For a *d*-dimensional dynamic system, there are *d* LEs as LE1 ≥ LE2 ≥ ... ≥ LEd. When LE1 > 0, namely, the system exhibits chaos; if LE1 > 0, and LE2 > 0, it exhibits hyperchaos. When LE1 = 0, the system is periodic or quasi-periodic, and when LE1 > 0, the system is unstable. The fractal dimension D_{ky} can be expressed in terms of LEs:

$$D_{ky} = k + \frac{1}{|\lambda_{k+1}|}\sum_{i=1}^{k}\lambda_i$$

where k meets the following conditions: $\sum_{i=1}^{k}\lambda_i \geq 0$ and $\sum_{i=1}^{k+1}\lambda_i < 0$.

The LE spectrum allows numerical exploration of the system's evolution from stable or quasi-periodic states to chaos or hyperchaos. By adjusting the pump of the assembled system, chaotic (and hyperchaotic), stable, and quasi-periodic regions can be identified. Figures 13–15 show LE spectra for varying pump values in increments of 0.1 for each laser.

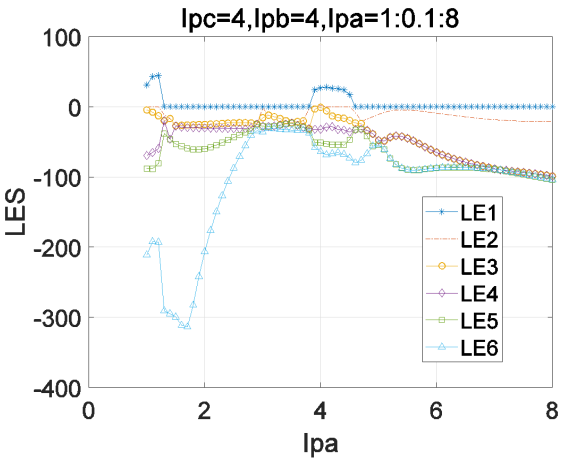

Fig. 13. LEs spectra *versus* the pump of laser A.

Figure 13 shows two chaotic regions: from I_{pa} = 1 to 1.3 and from I_{pa} = 3.9 to 4.5. A hyperchaotic region occurs from I_{pa} = 3.9 to 4.05, with two positive LEs of 26.8, and 1.28 at I_{pa} = 4. The remaining LEs are LE3 = 0, LE4 = –32.4, LE5 = –51.2, and LE6 = –64.1. Quasi-periodic regions are observed from 1.4 to 3.8 and from 4.6 to 8. Corresponding to the hyperchaotic region at I_{pa} = 4, the fractal dimension is D_{xy} = 9.49.

Figure 14 shows the stable region for I_{pb} = 1 to 1.8. Eight chaotic regions are observed: from 1.9 to 2.3, where the hyperchaotic region occurs between 2 and 2.2, with two positive LEs of 23.5 and 1.23 at I_{pb} = 2.1. The remaining LEs are LE3 = 0, LE4 = –14.2, LE5 = –27.1, and LE6 = –47.6. The quasi-periodic regions are observed: from I_{pb} = 4.1 to I_{pa} = 4.7, from 4.9 to 5; from 5.2 to 6.9, from 7.2 to 7.5, from 8.1 to 8.3, from 8.5 to 8.8 and from 9 to 10; corresponding to the hyperchaotic region on I_{pb} = 2.1, the fractal dimension is D_{xy} = 4.63.

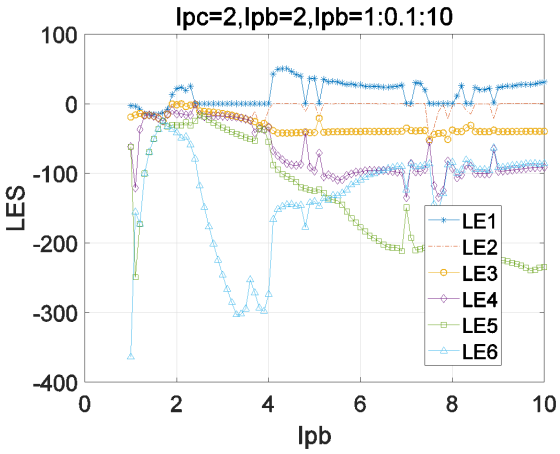

Fig. 14. LEs spectra *versus* the pump of laser B.

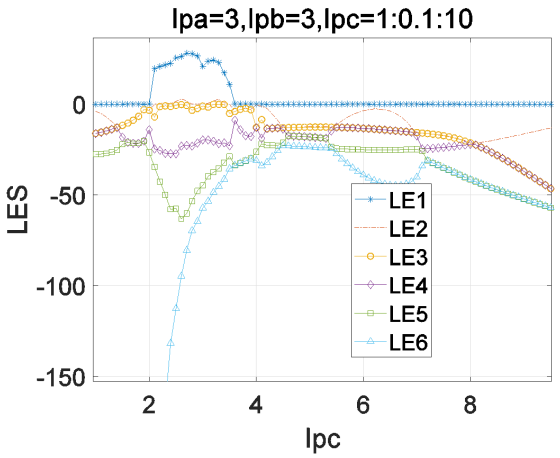

Fig. 15. LEs spectra *versus* the pump of laser C.

Figure 15 shows the chaotic region for I_{pc} = 2.2 to 3.5, with two hyperchaotic intervals from 2 to 2.8 and from 3 to 3.5. At I_{pc} = 2.6, the LEs are LE1 = 26.3, LE2 = 2.97, LE3 = 0, LE4 = –23.1, LE5 = –63.1, and LE6 = –94.7, with a fractal dimension D_{xy} = 4.2. At I_{pc} = 3.3, the LEs are LE1 = 23, LE2 = 2.97, LE3 = 0, LE4 = –22.5, LE5 = –35.4, and LE6 = –45.3, with D_{xy} = 4.04. All other intervals correspond to quasi-periodic regions.

4.3. The waveforms and power spectrum

The continuous oscillation behavior of the laser system produced lasing waves in each laser once the pump exceeded a threshold. These waves clearly exhibit one-periodic, quasi-periodic, chaotic, and hyperchaotic behaviors, corresponding to the emergence of different attractors, as depicted in Figs. 16–21. Chaotic and self-pulsing waves are associated with chaotic and periodic moving orbits in phase space, leading to the formation of strange attractors and monostable limit cycles. These diagrams provide insight into the distinctive dynamical features of the tri-ring laser oscillator.

Power spectrum analysis using the fast Fourier transform (FFT) complements this study by providing a quantitative valuable tool for investigating system dynamics and signals. The orbits and the time series wave are plotted, and the field signal is analyzed using the power spectrum, as shown in Figs. 16–21. These diagrams provide a detailed

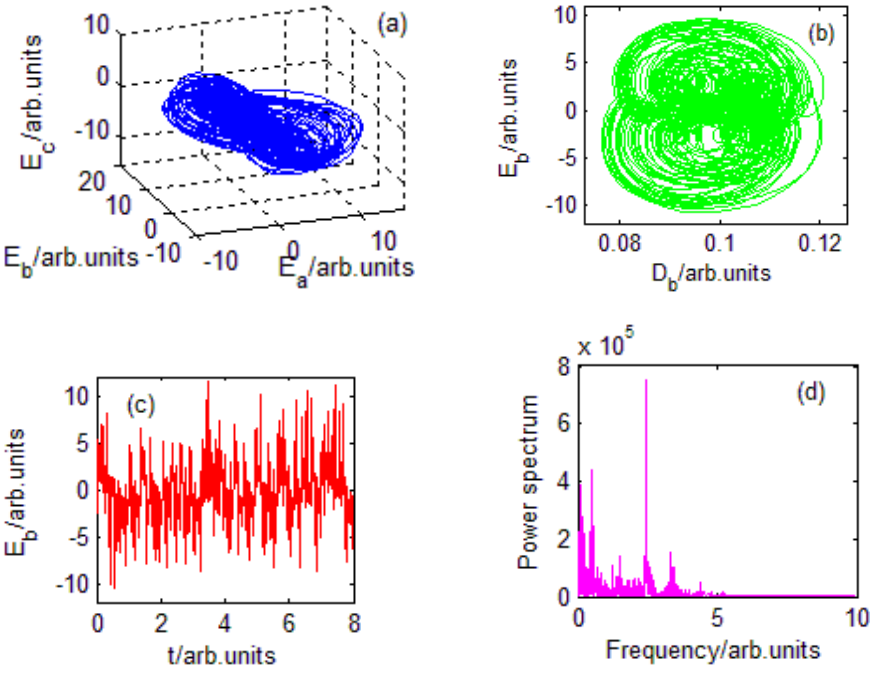

Fig. 16. Hyperchaos: (a) attractor for the system, (b) attractor for laser B, (c) waveform for laser B, and (d) power spectrum for laser B.

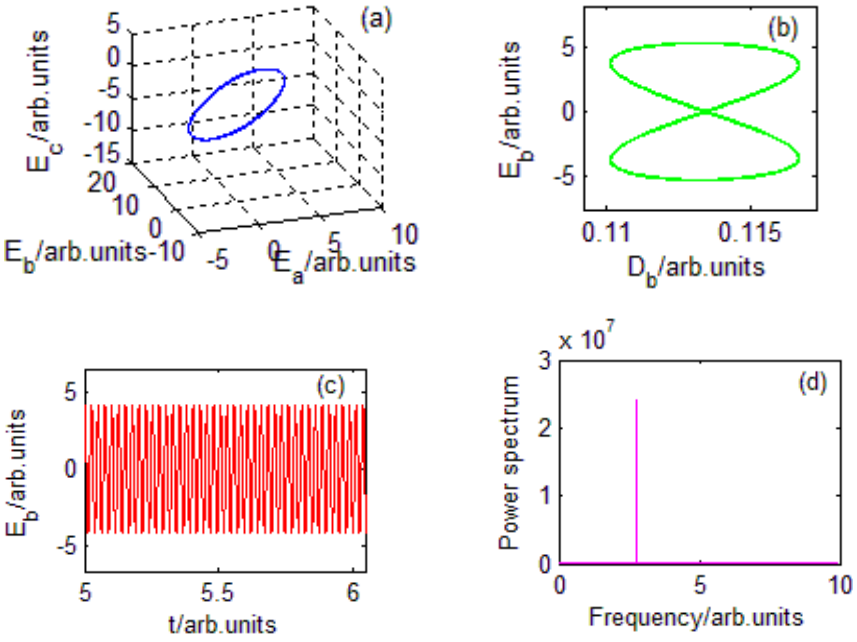

Fig. 17. One-period: (a) limit cycle for the system, (b) limit cycle for laser B, (c) self-pulsing for laser B, and (d) power spectrum for laser B.

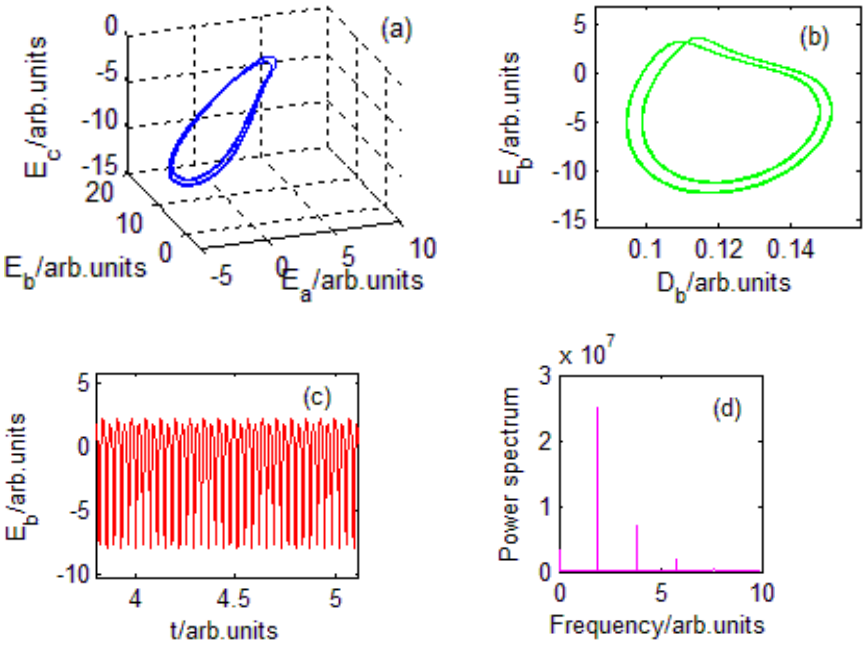

Fig. 18. Double-period: (a) cycle-2 for the system, (b) cycle-2 for laser B, (c) twin-pulsing for laser B, and (d) power spectrum for laser B.

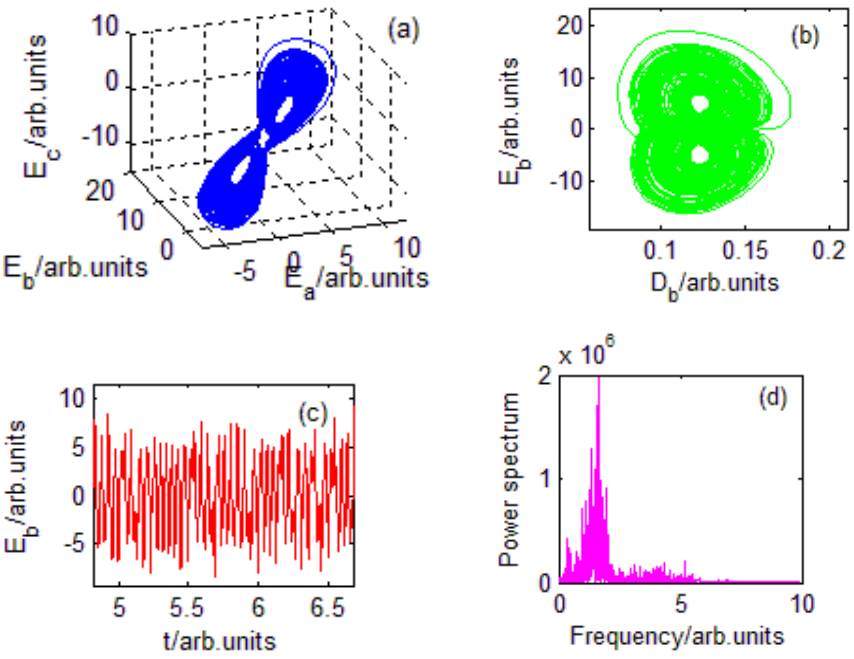

Fig. 19. Chaos: (a) attractor for the system, (b) attractor for laser B, (c) waveform for laser B, and (d) power spectrum for laser B.

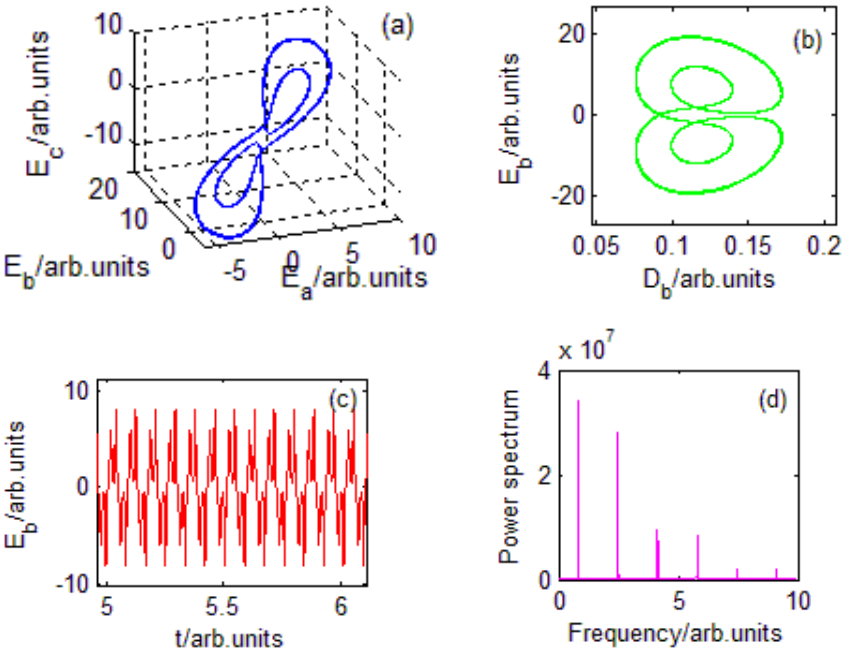

Fig. 20. Three-period: (a) cycle-3 for the system, (b) cycle-3 for laser B, (c) waveform for laser B, and (d) power spectrum for laser B.

visualization of the transitions from stable to hyperchaotic states and from chaos to quasi-periodicity.

Using parameters corresponding to Figs. 8 and 14, we examined the system's response to variations in I_{pb}. At $I_{pb} = 1.8$, the oscillation of the system decays to a stable state (LE1 = –7.87) due to low pump power. Laser A stabilizes at $E_a = 2.4083$, laser B stabilizes at $E_b = -2.1078$, and laser C stabilizes at $E_c = -2.3265$. When I_{pb} increased to 2, the pump was sufficient to stimulate a second oscillation, leading to continuous oscillation and hyperchaos (LE1 = 21.82, LE2 = 0.14, LE3 ≈ 0, see Fig. 8(b)), as shown in Fig. 16. The hyperchaotic wave is accompanied by hyperchaotic and periodic moving orbits in dynamic phase space, with strange attractors displaying ergodicity (see Figs. 16(a) and (b)). The stochastic waveform (Fig. 16(c)) transforms into a hyperchaotic solution with a broadband power spectrum (Fig. 16(d)), showing numerous frequency peaks with varying amplitudes.

As the pump value is further increased to $I_{pb} = 3$, a Hopf bifurcation occurs in the system (LE1 = 0, also see Fig. 8(b)), and self-pulsing is accompanied by periodic moving orbits in dynamic phase space. This leads to the transformation of the limit cycle into a one-periodic solution, characterized by a commensurate frequency, as shown in Fig. 17.

As the pump value is further increased to $I_{pb} = 4$, a double-periodic bifurcation occurs (LE1 = 0), and the twin-pulsing behavior is accompanied by double-periodic moving orbits in dynamic phase space. This results in a double-cycle transforming into a double-periodic solution characterized by commensurate frequencies, as shown in Fig. 18.

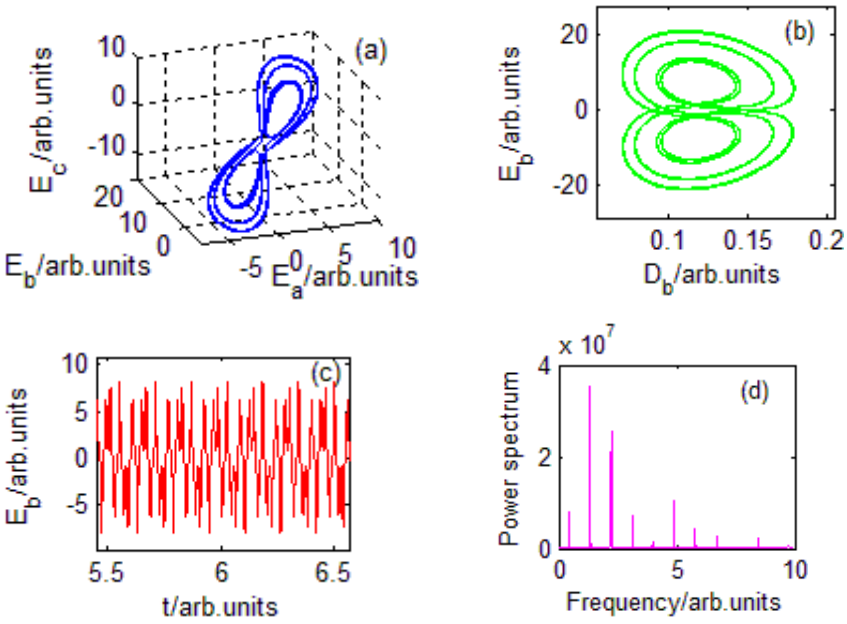

Fig. 21. Four-period: (a) cycle-4 for system, (b) cycle-4 for laser B, (c) waveform for laser B, and (d) power spectrum for laser B.

A continued increase of the pump level I_{pb} eventually leads to the destruction of the quasi-period, resulting in chaos. With the pump increased to $I_{pb} = 5$, a stochastic wave (chaos) occurs in the system (LE1 = 36.4, LE2 = 0), accompanied by chaotic moving orbits in dynamic phase space, which leads to the transformation of the stochastic oscillation into a chaotic solution characterized by the widened frequency spectrum shown in Fig. 19.

A continued increase of the pump level I_{pb} leads to the decay of the chaos, resulting in a direct transition away from chaos and entering three-period. As the pump increases to $I_{pb} = 7.5$, the chaotic behavior decays, and the system transitions into a three-periodic state (LE1 = 0). The three-periodic moving orbits in phase space correspond to a three -periodic waveform, characterized by commensurate frequencies, shown in Fig. 20.

When the pump reaches $I_{pb} = 8.4$, the system exhibits a four-periodic waveform (LE1 = 0), with four-periodic moving orbits in phase space. This results in a four-periodic solution characterized by commensurate frequencies, as shown in Fig. 21.

5. Conclusions

In our study, we created a hyperchaotic tri-ring Er-doped fiber laser system, assembled from three single-ring Er-doped fiber lasers and two couplers. Using a six-dimensional mathematical model that accounts for the laser fields and population inversions of all three lasers, we extensively analyzed the system's dynamics along the route from stability to chaos and hyperchaos in each laser ring. Our investigation employed multiple tools, including time-series wave analysis, bifurcation diagrams, power spectra, fractal dimensions, and LEs. We focused on the exploration paths to chaos and hyperchaos, identifying one-period, quasi-periodic, chaotic, and hyperchaotic regimes depending on system parameters. Notably, we observed the coexistence of chaos and hyperchaos within specific parameter ranges.

Our numerical analysis traced the system's evolution from a stable state through quasi-periodic dynamics to chaos and hyperchaos, revealing bifurcation scenarios as system parameters were varied. By adjusting the pump levels of individual laser rings, we identified chaotic, stable, and double-periodic bifurcation regions. Similarly, altering the coupling strength between two rings produced two chaotic regions and a double-periodic regime, while varying the gain coefficient and decay rate revealed additional chaotic, stable, and double-periodic regions. Each single-ring laser subsystem maintained its intrinsic nonlinear dynamics, and the assembled tri-ring system exhibited rich collective behaviors, including quasi-periodic motion, bifurcation, chaos, and hyperchaos. LEs were used to diagnose dynamic behavior, and fractal dimensions characterized the geometric structure of the resulting attractors.

We also found that the hyperchaotic waves were accompanied by hyperchaotic and periodic moving orbits in dynamic phase space, with strange attractors exhibiting ergodicity. The real-time waveforms demonstrated both complexity and randomness, and the hyperchaotic signals produced wide-band spectra, as evidenced by numerous frequency peaks with varying amplitudes in the power spectrum.

Mathematically, we derived the stable-field functions for each single-ring laser as a function of the pump, displaying a set of stable output distributions for the three lasers. Theoretical analysis of system instability using three sets of cubic relation expressions, supported by nonlinear function curves, confirmed the possible existence of twin-scroll strange attractors in each laser ring and a hyper-scroll strange attractor in the assembled tri-ring laser system. The hyper-scroll strange attractor was diagnosed as hyperchaotic through LE analysis, in agreement with our numerical result.

The assembled tri-ring laser system demonstrates significant potential for application in the fields of fiber laser technology, laser chaos research, optical secure communication, optical random signal generation, and laser radar systems.

Acknowledgment
This work was supported by the key subject of Jiangsu Province and Nanjing Key Laboratory, China. The authors thank H. J. Wang for helpful discussions.

Conflicts of interest
The authors declare no conflicts of interest.

References

[1] Guo X.M., Liu T., Wang L.J., Fang X., Zhao T., Virte M., Guo Y.Q., *Evaluating entropy rate of laser chaos and shot noise*, Optics Express **28**(2), 2020: 1238-1248. https://doi.org/10.1364/OE.380213

[2] Chang D., Zhong Z.Q., Tang J.M., Spencer P.S., Hong Y.H., *Flat broadband chaos generation in a discrete-mode laser subject to optical feedback*, Optics Express **28**(26), 2020: 39076-39083. https://doi.org/10.1364/OE.413674

[3] Chiu C.P., Jiang X.W., Chang K.C., Wei M.D., *Chaos and extreme events in an azimuthally polarized Nd:$GdVO_4$ laser with pump modulation*, Optics Letters **42**(3), 2017: 423-426. https://doi.org/10.1364/OL.42.000423

[4] Sunada S., Shinohara S., Fukushima T., Harayama T., *Signature of wave chaos in spectral characteristics of microcavity lasers*, Physical Review Letters **116**(20), 2016: 203903-203908. https://doi.org/10.1103/PhysRevLett.116.203903

[5] Sciamanna M., Shore K.A., *Physics and applications of laser diode chaos*, Nature Photonics **9**(3), 2015: 151-162. https://doi.org/10.1038/nphoton.2014.326

[6] Tsay H.L., Wang C.Y., Chen J.D., Lin F.Y., *Generations of chaos-modulated pulses based on a gain -switched semiconductor laser subject to delay-synchronized optical feedback for pulsed chaos lidar applications*, Optics Express **28**(16), 2020: 24037-24046. https://doi.org/10.1364/OE.399609

[7] Wang D., Wang L.S., Li P., Zhao T., Jia Z.W., Gao Z.S., Guo Y.Y., Wang Y.C., Wang A.B., *Bias current of semiconductor laser: An unsafe key for secure chaos communication*, Photonics **6**(2), 2019: 59. https://doi.org/10.3390/photonics6020059

[8] Chemo Y.K., *Laser-based optoelectronic generation of narrowband microwave chaos for radars and radio-communication scrambling*, Optics Letters **42**(17), 2017: 3431-3434. https://doi.org/10.1364/OL.42.003431

[9] Roy A., Misra A.P., Banerjee S., *Chaos-based image encryption using vertical-cavity surface-emitting lasers*, Optik **176**, 2019: 119-131. https://doi.org/10.1016/j.ijleo.2018.09.062

[10] Hu D.W., Wang F., Li J,C., Deng T., Wu J.G, Wu Z.M., Xia G.Q., *Wideband chaotic comb source using a weak-resonant-cavity Fabry-Perot laser diode subject to optical feedback for parallel random number generation*, Chaos, Solitons & Fractals **188**, 2024: 115458. https://doi.org/10.1016/j.chaos.2024.115458

[11] LIU S.Q., JIANG N., ZHAO A.K., ZHANG Y.Q., QIU K., *Secure optical communication based on cluster chaos synchronization in semiconductor lasers network*, IEEE Access **8**, 2020: 11872-11879. https://doi.org/10.1109/ACCESS.2020.2965960
[12] XUE C.P., XIA Y.K., CHEN W., GU P., ZHANG Z., *Physical-layer security of optical communication based on chaotic optical encryption without an additional driving signal*, Optics Letters **48**(10), 2023: 2611-2614. https://doi.org/10.1364/OL.487627
[13] NGUIMDO R.M., KHODER M., DANCKAERT J., VAN DER SANDE G., VERSCHAFFELT G., *Fast phase response and chaos bandwidth enhancement in semiconductor lasers subject to optical feedback and injection*, Optics Letters **39**(20), 2014: 5945 -5948. https://doi.org/10.1364/OL.39.005945
[14] YAN S.L., *Theory of stability and bifurcation in a multi-quantum well laser with opto-electronic delayed feedback*, Optics and Laser Technology **44**(1), 2012: 83-91. https://doi.org/10.1016/j.optlastec.2011.05.024
[15] YAN S.L., *Study of bistability and hyperchaos in a coupled class-B laser system*, Electronics Letters **60**(24), 2024: e70119. https://doi.org/10.1049/ell2.70119
[16] XIANG S., PAN W., YAN L., LUO B., ZOU X., JIANG N., WEN K., *Influence of polarization mode competition on chaotic unpredictability of vertical-cavity surface-emitting lasers with polarization-rotated optical feedback*, Optics Letters **36**(3), 2011: 310-312. https://doi.org/10.1364/OL.36.000310
[17] WU J.G., ZHAO L.J., WU Z.M., LU D., TANG X., ZHONG Z.Q., XIA G.Q., *Direct generation of broadband chaos by a monolithic integrated semiconductor laser chip*, Optics Express **21**(20), 2013: 23358-23364. https://doi.org/10.1364/OE.21.023358
[18] XIANG S., PAN W., ZHANG L., WEN A., SHANG L., ZHANG H., LIN L., *Phase-modulated dual-path feedback for time delay signature suppression from intensity and phase chaos in semiconductor laser*, Optics Communications **324**, 2014: 38-46. https://doi.org/10.1016/j.optcom.2014.03.017
[19] KINGSTON S.L., BALCERZAK M., DANA S.K., KAPITANIAK T., *Transition to hyperchaos and rare large-intensity pulses in Zeeman laser*, Chaos **33**(2), 2023: 023128. https://doi.org/10.1063/5.0135228
[20] DROSTE S., YCAS G., WASHBURN B.R., CODDINGTON I., NEWBURY N.R., *Optical frequency comb generation based on erbium fiber lasers*, Nanophotonics **5**(2), 2016: 196-213. https://doi.org/10.1515/nanoph-2016-0019
[21] ZHAO L., LI D., LI L., WANG X., GENG Y., SHEN D., SU L., *Route to larger pulse energy in ultrafast fiber lasers*, IEEE Journal of Selected Topics in Quantum Electronics **24**(3), 2018: 8800409. https://doi.org/10.1109/JSTQE.2017.2771739
[22] MA M.X., HU Z.L., XU P., WANG W., HU Y.M., *Experimental study on chaos generation in an all-fiber erbium-doped fiber ring laser with a Mach-Zehnder interferometer*, Chinese Optics Letters **12**(8), 2014: 081403.
[23] WU Q., OKABE Y., SUN J., *Investigation of dynamic properties of erbium fiber laser for ultrasonic sensing*, Optics Express **22**(7), 2014: 8405-8419. https://doi.org/10.1364/OE.22.008405
[24] LUO L.G., CHU P.L., *Optical secure communications with chaotic erbium-doped fiber lasers*, Journal of the Optical Society of America B **15**(10), 1998: 2524-2530. https://doi.org/10.1364/JOSAB.15.002524
[25] LUO L., TEE T.J., CHU P.L., *Chaotic behavior in erbium-doped fiber-ring lasers*, Journal of the Optical Society of America B **15**(3), 1998: 972-978. https://doi.org/10.1364/JOSAB.15.000972
[26] DANIE J., COSTA J-M., LEBOUDEC P., STEPHAN G., SANCHEZ F., *Generalized bistability in an erbium -doped fiber laser*, Journal of the Optical Society of America B **15**(4), 1998: 1291-1294. https://doi.org/10.1364/JOSAB.15.001291
[27] ARGYRIS A., SYVRIDIS D., LARGER L., ANNOVAZZI-LODI V., COLET P., FISCHER I., GARCÍA-OJALVO J., MIRASSO C.R., PESQUERA L., SHORE K.A., *Chaos-based communications at high bit rates using commercial fiber-optic links*, Nature **438**(7066), 2005: 343-346. https://doi.org/10.1038/nature04275
[28] KUMAR G., VIJAYA R., *Control of dynamics in a loss-modulated erbium-doped fiber ring laser*, Journal of the Optical Society of America B **34**(3), 2017: 574-582. https://doi.org/10.1364/JOSAB.34.000574

[29] YAN S.L., *Study of chaos-control of a dual-ring erbium-doped fiber laser using parameter method*, Journal of Optical Communications **42**(1), 2021: 9-15. https://doi.org/10.1515/joc-2018-0021

[30] YAN S.L., *Study on the method of controlling chaos in an Er-doped fiber dual-ring laser via external optical injection and shifting optical feedback light*, Chaos 17(1), 2007: 013106. https://doi.org/10.1063/1.2424894

[31] SHEN K., WANG R., *Synchronization of chaotic systems modulated by another chaotic system in an erbium-doped fiber dual-ring laser system*, IEEE Journal of Quantum Electronics **37**(8), 2001: 960-963. https://doi.org/10.1109/3.937385

[32] YAN S.L., *Study of hyperchaos resulting from an erbium-doped fibre three-ring laser system*, Electronics Letters **58**(7), 2022: 288-289. https://doi.org/10.1049/ell2.12426

[33] YAN S.L., *Displays of high-grade hyperchaos and bi-stability in an erbium-doped fiber three-ring mutual-coupled laser*, Optics Communications **577**, 2025: 131338. https://doi.org/10.1016/j.optcom.2024.131338

[34] DE LA TORRE J.O.E., GARCÍA-LÓPEZ J.H., JAIMES-REÁTEGUI R., HUERTA-CUELLAR G., ABOITES V., PISARCHIK A.N., *Route to chaos in a unidirectional ring of three diffusively coupled erbium-doped fiber lasers*, Photonics **10**(7), 2023: 813. https://doi.org/10.3390/photonics10070813

[35] YAN S.L., WANG H.J., *Bifurcation and hyperchaos in a tri-ring Er-doped fiber laser*, Proceedings of the SPIE, Vol. 13965, International Conference on Optics, Electronics, and Communication Engineering (OECE 2025), 2025: 1396545. https://doi.org/10.1117/12.3089808

Received July 17, 2025
in revised form September 24, 2025